Rare Earth Elements of the Arima Spring Waters, Southwest Japan: Implications for Fluid – Crust Interaction during Ascent of Deep Brine

Hitomi Nakamura[1,2*], Kotona Chiba[2], Qing Chang[1], Shunichi Nakai[3], Kohei Kazahaya[4] and Hikaru Iwamori[1,2]

[1]*Japan Agency for Marine–Earth Science and Technology, 2-15 Natsushima-cho, Yokosuka-shi, Kanagawa 237-0061, Japan*
[2]*Department of Earth and Planetary Sciences, Tokyo Institute of Technology, 2-12-1 Ookayama, Meguro-ku, Tokyo 152-8551, Japan*
[3]*Earthquake Research Institute, University of Tokyo, 1-1-1 Yayoi, Bunkyo-ku, Tokyo 113-0033, Japan*
[4]*Geological Survey of Japan, AIST, 1-1-1 Higashi, Tsukuba, Ibaraki 305-8567, Japan*

Abstract

Rare earth elements (REEs) of the eight Arima spring waters in southwest Japan, including Arima-type brine that represents a specific type of deep-seated brine of up to 6 wt.% NaCl in the non-volcanic fore-arc region, have been investigated in order to discuss their upwelling processes and origins. We found four distinct patterns of REE composition of the spring waters within the Arima area of ~1 km², based on which two sources for REEs and two aquifers are inferred in the modification of the original deep-seated brine composition. On the basis of the REEs and isotopic compositions of the original deep brine, one of the two sources is thought to be slab-derived fluid dehydrated from the subducted Philippine Sea slab beneath the Arima area, represented by the 'Kinsen' hot spring water [1]. The convex-down REE pattern of most Arima spring waters, except for 'Kinsen' and 'Tansansen', suggests the presence of an oxidizing aquifer deeper than 160 m that causes co-precipitation of REEs with oxyhydroxides. CO_2 and He degassed from this aquifer flux the overlying shallow aquifer less than ~50 m in depth, producing highly carbonated water such as 'Tansansen' water that was originally derived from meteoric water. The carbonated water may dissolve a significant amount of REEs to the 'Tansansen' spring water from the host rocks, which are possibly silicic igneous rocks with Eu-negative anomalies. The four types of REE patterns with a wide concentration range, therefore, provide invaluable information concerning fluid–crust interaction during ascent of the deep brine.

Introduction

Arima-type brine is non-volcanic hot spring water with high salinity found in a fore-arc region with no Quaternary volcanism [2]. This water has been geochemically characterized by a high Cl content at ~40000 ppm and specific O–H isotopic ratios that are similar to magmatic/metamorphic thermal waters. Despite its occurrence in a non-volcanic region, this water is distinct from meteoric water or buried sea water [2-4]. It also shows high $^3He/^4He$ ratios comparable or close to the mantle value and characteristic ratios of both stable and radiogenic isotopes (i.e., H, C, O, Sr, Nd, and Pb) that indicate slab-fluid derived from the subducted Philippine Sea Plate (PHS), suggesting a deep origin of the brine [1,5-7].

Arima springs in southwest Japan (Figures 1, 2A and 2B), the type locality of Arima-type brine, consist of hot springs (≧25°C) and associated cold springs (<25°C) including highly carbonated water. These springs generally exhibit a wide O–H isotopic range, which can be explained by mixing of meteoric waters and the deep brine component [3,4,7]. δ18O is clearly correlated with δD, forming a straight mixing line between the meteoric water and the predicted slab-fluid generated by dehydration of PHS at ~50 km depth beneath the Arima area [7] (Figure 3A). The isotopic ratios also constitute linear variations with major solute elements such as Cl and Na (Figures 3B-3D), upon which the composition of the deep brine component has been estimated [4,7].

The deep-seated brine is relatively well characterized, as previously mentioned. It is thought to ascend along faults such as Atago-yama and Tenjin-yama faults associated with large tectonic lines such as the Arima–Takatsuki Tectonic Line (ATTL), as shown in Figure 2A, without undergoing significant geochemical modification [7,8]. However, the mechanism of encounter between the deep brine and the shallow meteoric waters to be mixed remains poorly understood.

In this study, we aim to constraining the geochemical processes at such shallow parts in which the deep component is mixed with the meteoric waters. For this objective, we analyze and utilize rare earth elements (REEs), particularly lanthanoids, of Arima spring waters. The geochemical behavior and partitioning of REEs between solid and fluid are sensitive to temperature, fO_2, fCO_2, and pH and may provide key information on the mixing processes at the shallow level where temperature, volatile fugacity, and pH are potentially variable [9,10]. First, we provide new data on REEs for Arima spring waters and compare the results with major solute elements and O–H isotopes, resulting in the identification of several types of spring water [9,10]. On the basis of these variations, we discuss the geochemical processes and mechanism related to the mixing of deep brine with meteoric waters.

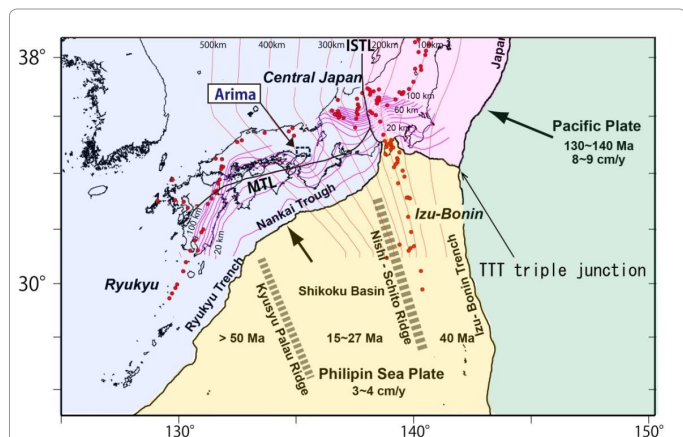## Geological and Tectonic Setting of the Studied Area

In the Arima region, spring waters occur in a narrow area of approximately 1 km² (Figure 2B) and show compositional variation in major solute elements and gases [7]. These springs appear to upwell through the ATTL and subsidiary faults striking NW–SW or NW–SE with dextral slip associated with the Median Tectonic Line formed in the late mid-Miocene in the southwest Japan arc (Figure 2A) [11,12].

Figure 1: Tectonic setting in Japan and location of the study area. The map shows the distribution of Quaternary volcanoes (red circles) and the geometry of the subducting Pacific and Philippine Sea slabs relative to the Itoigawa–Shizuoka Tectonic Line (ISTL) and the Median Tectonic Line (MTL). The pinkish contour lines indicate the depth of the upper surface of the Pacific slab (50 to 300 km depth with 50 km intervals), whereas the purplish contour lines indicate that of the Philippine Sea slab (10 to 200 km depth with 10 km intervals). The aseismic parts are shown by the dotted line.
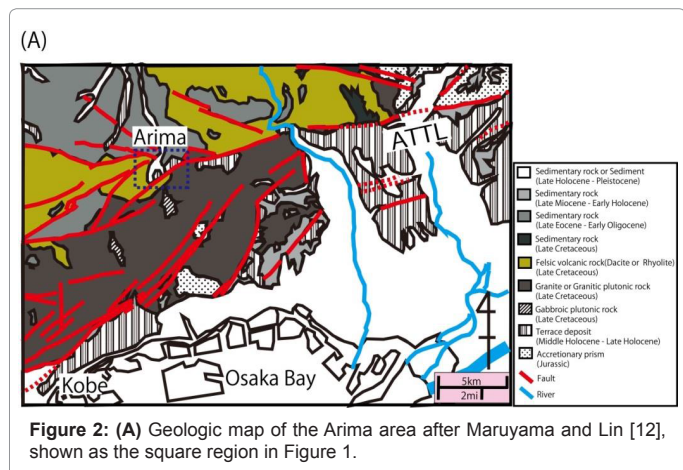
Figure 2: (A) Geologic map of the Arima area after Maruyama and Lin [12], shown as the square region in Figure 1.

The average slip rate for the eastern range-front segment of the tectonic line during the late Quaternary period is estimated to be 0.5–1.5 mm/year dextrally and 0.1–0.8 mm/year vertically [13]. The southwest Japan arc is associated with two oceanic plates, the Pacific plate and the PHS, which subduct beneath the area from the east at 9 cm/year and from the southeast at 4 cm/year, respectively. The slab surface depth beneath the Arima area is ~400 km for the Pacific slab but 50–80 km for the PHS, showing a large uncertainty [14,15]. Despite this active subduction, a Quaternary volcano has not formed in this region because the Pacific slab is too deep and the PHS is too shallow to fulfill the physiochemical conditions for arc magma generation (Figure 1) [16].

As shown in the geological map of this area (Figure 2A), the basement around the Arima area is composed of late Cretaceous felsic volcanic rocks such as rhyolite of the Arima Group, granitic rocks such as Rokko granite, and late Eocene to early Oligocene non-marine sedimentary rocks with rhyolitic tuff layers of the Kobe Group [17]. The Arima Group directly covers the Rokko granite south of the ATTL and the sedimentary rhyolitic rocks north of the ATTL in the Arima area [18].
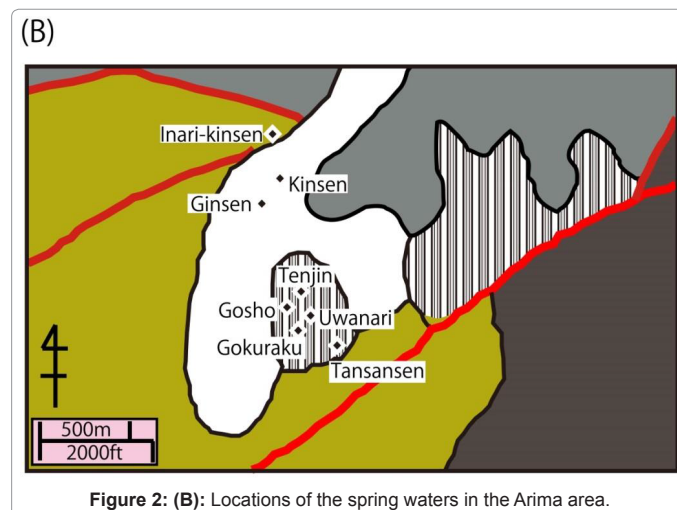
Chemical Analysis

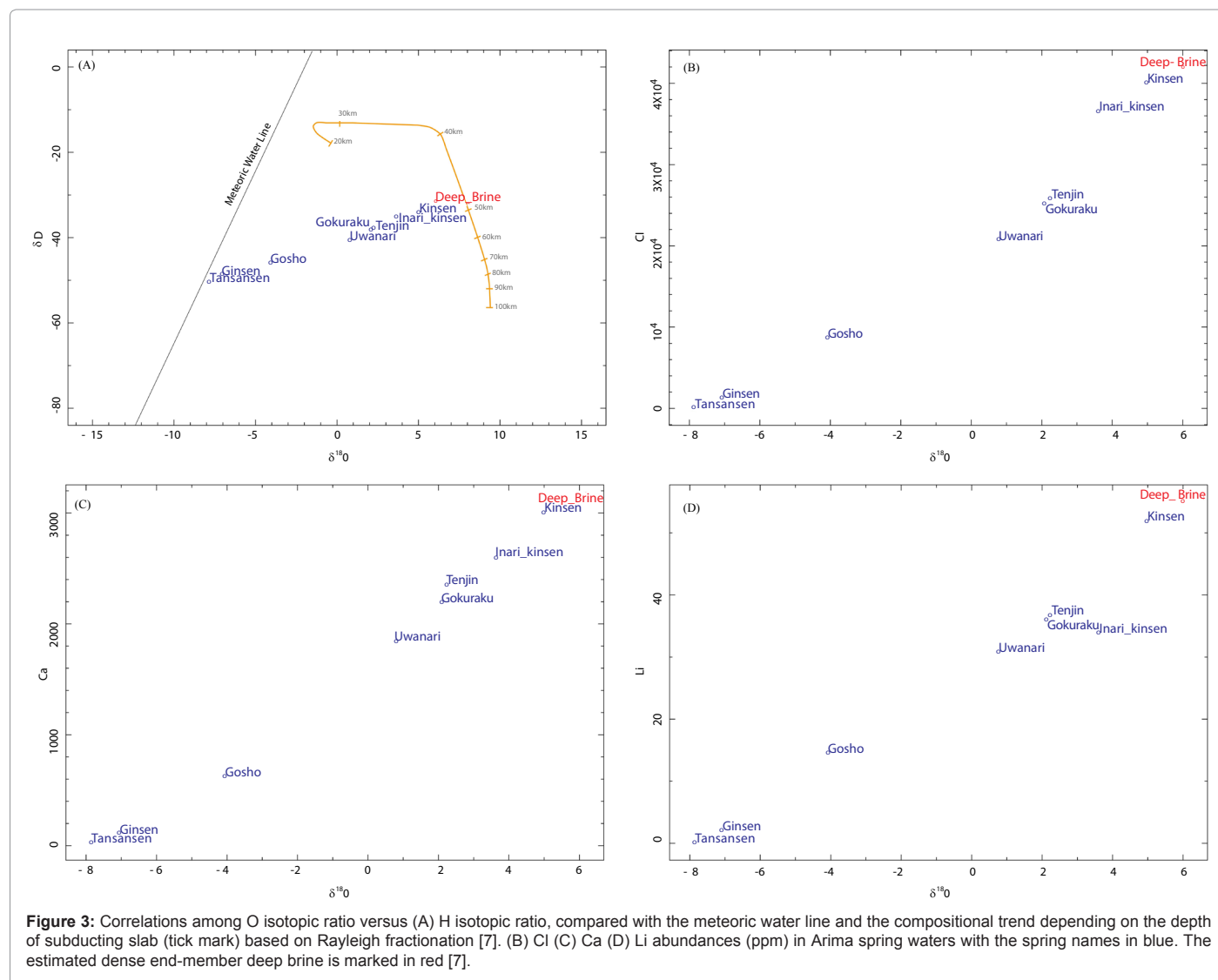### Sample description of Arima spring waters

The hot spring sources in the Arima area have been characterized by NaCl and hydrocarbon contents in addition to O–H–He isotopic composition [4,7], in most of which (Ginsen, Gokuraku, Gosho, Inari-Kinsen, Kinsen, Tansansen, Tenjin, and Uwanari waters) were investigated to understand their generation processes in this study (Figure 2B). During the dry season in December 2010, we collected 10 L samples of each of these waters directly from the well pipe before the water is pooled in tanks to be oxidized for commercial use. The Japanese names of these spring waters carry deep meanings. For example, "Kinsen" means gold-colored hot spring source, and "Tansansen" means high abundance of CO_2. Kusuda et al. [7] analyzed 12 solute elements/components and the isotopic ratios of H, He, C, and O in these spring waters and gases. Their results indicate a large range of elements, particularly in Cl (14–40,000 ppm) and hydrocarbon (12–1300 ppm) contents, adding to the wide range of O–H isotopic compositions. The He isotopic ratio has a smaller gap among these samples at 2–10 ($\times 10^{-6}$), which is similar to the mantle value, indicating deep origin [7]. The Li/Cl ratios for the spring waters are almost stable with a maximum of approximately 0.001, indicating a signature of Arima-type brine as suggested by Kazahaya et al. [19]. An exception is 'Tansansen' water, which has twice that value. These chemical signatures of spring waters can be explained by the mixing of meteoric water with slab-derived fluid of the PHS thought to be dehydrated at 50–80 km depths. The spring water with the lowest O–H isotopic composition close to a meteoric signature is identified with the lowest content of Cl and other cations such as Na, Ca, Br, Li, and Sr and the highest He^3/He^4 ratio, named as "Tansansen" which means saturated water with isolated carbonaceous gas. That with an opposite signature close to the end-member of 'Deep Brine', with the highest Cl and a higher He^3/He^4 ratio is identified as "Kinsen" (Figures 3A-3D). Other spring waters with moderate Cl and cation contents plotted between 'Tansansen' and 'Kinsen'.

Analytical method for REE composition in high-salinity brine

The high-salinity and solute elements in the brine may interfere with quantitative analysis of the REEs due to the matrix effect. In case of several water samples contained visible particles, we dissolved the visible particles in water by using acid. In order to consider the matrix effect with high-salinity conditions, we applied

Figure 2: (B): Locations of the spring waters in the Arima area.

Figure 3: Correlations among O isotopic ratio versus (A) H isotopic ratio, compared with the meteoric water line and the compositional trend depending on the depth of subducting slab (tick mark) based on Rayleigh fractionation [7]. (B) Cl (C) Ca (D) Li abundances (ppm) in Arima spring waters with the spring names in blue. The estimated dense end-member deep brine is marked in red [7].

the standard addition method for solutions with strong matrix effects with 0.4 ml addition of XSTC-1 (SPEX CertiPrep Co. Ltd., USA) by 0.001 ppb, 0.01 ppb, and 0.1 ppb in each 2.0 ml of each sample [20]. The samples were carefully diluted with ultra-pure water (>18.3 MΩ milli-Q water, Millipore Corporation, Japan) by using a weight scale in a class 100 clean room to minimize possible environmental contamination. The ICP-MS (iCAP-Qc, ThermoFisher Scientific) analysis was conducted at the Japan Agency for Marine–Earth Science and Technology (JAMSTEC). The analytical conditions were constantly monitored by using a standard tuning solution and diluted 5% HNO_3 acid solution. The reproducibility standard deviation (RSD) was approximately 2–4% for five repeated data acquisitions, indicating analysis stability [21]. The detection limit was 0.1 ppt. It should be noted that Eu, Nd, Sm, and Gd were quantitatively re-calculated after being combined with ^{135}Ba for correction due to significant interference from Ba oxides, which enabled us to discuss the Eu-anomaly. The most significant interference on REEs signals come from Ba polyatomic ions, because Ba is one of the highest abundant elements in the brine samples. We carefully investigated the formation of these polyatomic ions in ICP-MS measurement by analyzing pure Ba solution, and estimated

for typical brine waters that Ba interfering ions contributed to La, Ce, Nd, Sm, Eu and Gd raw signals for 92%, 24%, 48%, 78%, 96% and 75%, respectively. Pr is free from any of Ba oxide and hydroxide interference which exist farthest to Gd. Intra REEs interfering, e.g., PrO, NdO and SmO overlapping on MREE and HREE signals, were found less than 2.7% (mostly <1%), thus ignorable for this study.

Results

REE abundances and patterns of Arima spring waters

The analytical results of REEs are listed in Table 1. The REE compositions are plotted in Figure 4 as spidergram patterns normalized by depleted mid-ocean ridge basalt (MORB) mantle (DMM). The REE abundances of Arima spring waters are approximately three to five times lower than those of DMM. We have detected four distinct patterns in these spring waters: (i) a flat pattern with a negative Eu-anomaly, represented in the figure by the light blue line; (ii) a slightly convex-down pattern of increasing concentration toward both the left and right, indicating light REEs (LREEs) and heavy REEs (HREEs), respectively, associated with a moderately positive Eu-anomaly (blue line); (iii) a strongly convex-down pattern with a strong positive Eu-

anomaly (black line); and (iv) a slightly convex-down pattern with a moderately positive Eu-anomaly and a negative Ce-anomaly (dark blue line). Except for 'Tansansen' (light blue line), which is a highly carbonated cold spring, all spring waters have positive Eu-anomalies; 'Kinsen' (blue line) shows the highest REE content. Among 'Ariake', 'Gosho', 'Gokuraku', 'Tenjin', and 'Uwanari', the five samples classified as (iii), the degree of positive Eu-anomaly increased for samples with a stronger convex-down pattern. 'Kinsen', classified as (ii), maintained overall high concentrations for both LREEs and HREEs with a slightly convex-down pattern (Figure 4). 'Ginsen' (dark blue line), classified as (iv), is a cold spring exhibiting a relatively flat pattern and is in this sense similar 'Tansansen' (i). However, the former shows overall low concentrations (Figure 4).

Correlation of REEs and major solute elements

The solute major elements, Cl and Li abundances, and $\delta^{18}O$–δD–He isotopic ratios in the spring waters, the REEs of which are presented in Table 1, are summarized in Table 2 [7,22]. As previously mentioned, all spring waters are aligned along a single mixing line between the meteoric water and a dense end-member as the deep brine component (Figures 3A-3D), which approximately corresponds to a slab-derived fluid dehydrated at an approximately 50 km depth [7]. 'Kinsen' has high O and H isotopic ratios close to the dense end-member, indicating less involvement of meteoric water, whereas the two cold springs, 'Tansansen' and 'Ginsen', have nearly the same $\delta^{18}O$ and δD as the meteoric water (Figure 3A). However, as shown in Table 2, 'Tansansen', the highly carbonated cold spring water, has the highest $^3He/^4He$ ratio, indicating deep origin; 'Kinsen' also has a high ratio indicative of its mantle origin. Other springs are plotted along a mixing line between 'Tansansen' and air-saturated water [7]. It is also noted that no clear relationship is observed between dissolved HCO_3 and the major solute concentrations, particularly Cl, that represent the proportion of dense end-members involved in the samples (Figure 2 and Table 2).

Arima	La	Ce	Pr	Nd	Sm	Eu	Gd	Tb	Dy	Ho	Er	Tm	Yb	Lu	Dilution rate
Ginsen	0.2228	0.0093	0.0389	0.2089	0.0773	0.1467	0.0665	0.0161	0.1094	0.0411	0.1799	0.0429	0.3818	0.0769	10.3386
Gokuraku	2.0849	n.a.	0.0216	0.0299	0.1322	10.7723	0.3484	0.0576	0.0214	0.0051	0.0074	0.0474	0.7346	0.1454	1.0000
Gosho	0.4306	0.0013	0.0055	0.0113	0.0339	1.8843	0.0351	0.0061	0.0049	0.0014	0.0033	0.0043	0.0294	0.0099	1.0000
Inari-kinsen	18.7829	0.0062	0.0219	0.0115	0.0804	54.6893	0.3182	0.0301	0.0675	0.0184	0.0504	0.0422	0.2696	0.1118	9.6825
Kinsen	11.0772	5.2442	0.5676	2.5409	0.9609	27.8899	1.7651	0.3841	3.6653	0.8360	2.5692	0.3392	2.4161	0.2924	42.2693
Tansansen	4.1881	13.3532	1.9650	10.4090	2.7646	0.3982	4.2497	0.5709	4.1635	0.7909	2.6780	0.3121	2.2442	0.2057	49.9452
Tenjin	3.7923	n.a.	0.0300	0.0126	0.0244	30.1594	0.1479	0.0470	0.0628	0.0118	0.0107	0.0562	0.6806	0.3203	1.0000
Uwanari	1.0906	0.0705	0.0187	0.0599	0.0889	4.4356	0.0928	0.0162	0.0113	0.0038	0.0138	0.0162	0.0889	0.0421	1.0000

Table 1: Rare earth element (REE) abundances (ppb) of Arima spring waters. Abbreviation: n.a. = not analyzed.
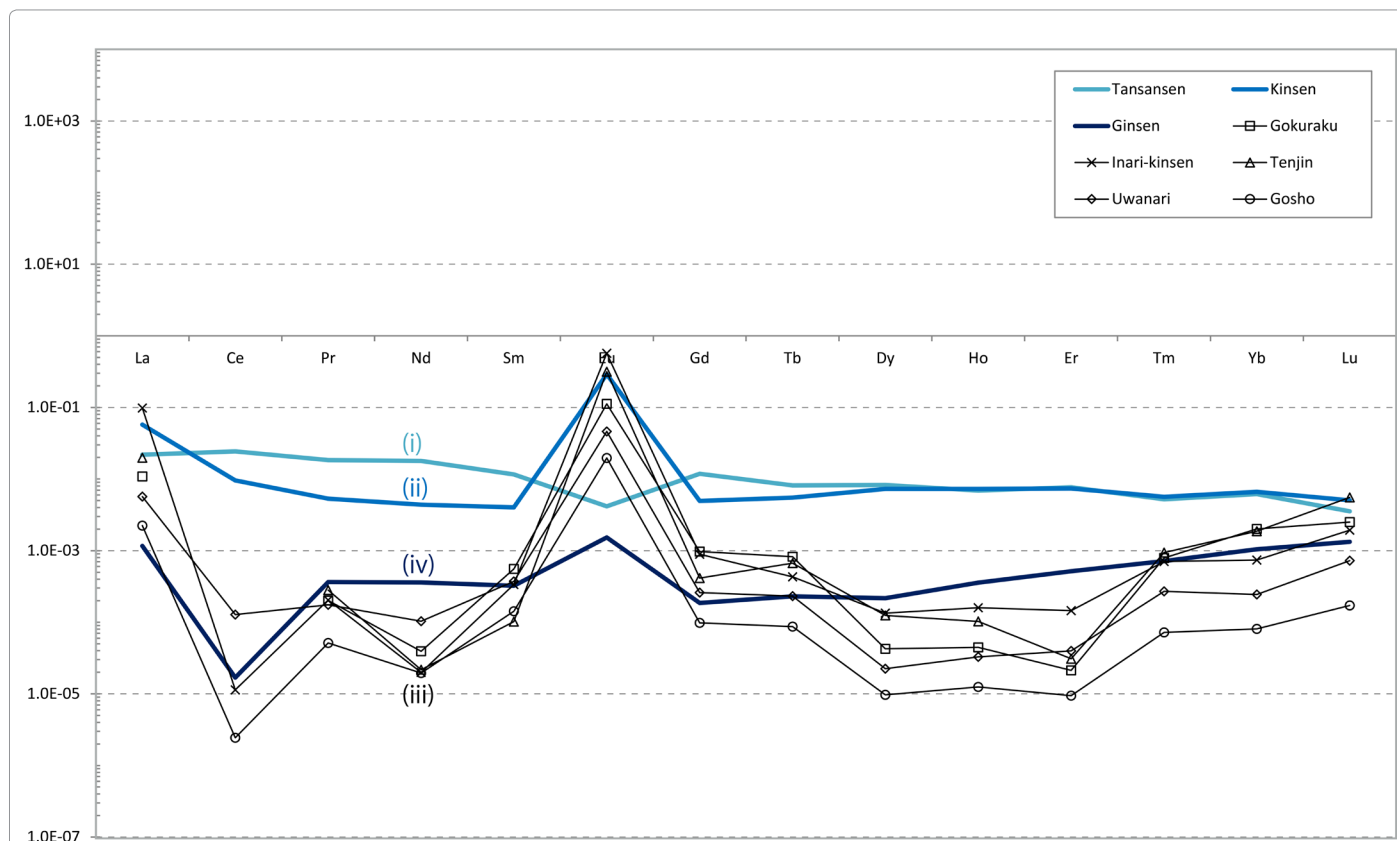

Figure 4: Depleted mid-ocean ridge basalt (MORB) mantle (DMM)-normalized rare earth element (REE) compositions of Arima spring waters analyzed in this study. The data are listed in Table 1.

Arima	Temperature (°C)	Depth (m)	Li (mg/L)	Cl (mg/L)	dD [SMOW]	$d^{18}O$ [SMOW]	$^3He/^4He$ [10^{-6}]	Li/Cl	HCO_3 (mg/L)	Ca (mg/L)	Sr (mg/L)
Ginsen	19.5	n.k.	2.08	1294	-48.56	-7.08	n.a.	0.0016	150	108	0.77
Gokuraku	95.3	240	35.78	25088	-38.15	2.07	3.26	0.0014	26	2192	43.49
Gosho	80.3	165	14.42	8742	-45.92	-4.09	3.84	0.0016	473	627	11.09
Inari-kinsen	32.2	n.k.	33.81	36602	-35.11	3.61	n.a.	0.0009	214	2598	93.94
Kinsen	29.2	n.k.	51.90	40033	-34.12	4.98	6.69	0.0013	1293	3006	80.35
Tansansen	19.1	40	0.03	14	-50.27	-7.88	10.29	0.0021	30	23	0.12
Tenjin	88.3	206	36.69	25828	-37.71	2.22	n.a.	0.0014	137	2356	41.01
Uwanari	88.3	187	30.76	20786	-40.50	0.77	3.34	0.0015	203	1845	37.08

Table 2: Major solute elements and isotopic composition discussed in this study. The data are from [7]. Abbreviation: n.k. = not known.

Concerning REE abundance in the spring waters, no clear correlation was noted with the Cl content and thus the proportion of deep brine component (Figures 5A-5C), implying that in addition to the mixing of the dense end-member with meteoric water, additional, independent processes controlling the REE content are required. The variability of the REE pattern shown in Figure 4 likely reflects such multiple processes (Figure 4). Because the dense, deep brine is thought to ascend through the fault system from depth without significantly reacting with the surrounding rocks [7], shallow crustal processes likely affect the REE behavior, where the dense brine encounters different environments with temperature and redox states distinct from those of the deep part. Such possibilities are discussed subsequently. As shown in Figure 5A-5C, 'Tansansen', being similar to the He systematics, again shows distinctly high REE concentrations despite a low Cl content. If 'Tansansen' is excluded, a broad and non-linear positive correlation exists between REE and Cl contents, with 'Kinsen' as an end-member of the highest concentration for most of the elements (Figure 5A-5C). This broad correlation is reflected in the REE pattern: 'Kinsen' plots at the highest concentrations, and the other five hot springs plot at lower concentrations with stronger convex-down patterns (Figure 4).

The convex-down pattern is related to the Eu-anomaly (Figure 4). In this section, we examine the relationship between the major solute elements and Eu abundance as shown in Figure 6A-6C. The behavior of Eu appears to be coupled with that of Cl, Ca, and Sr, although two broadly linear trends consisting of relatively cold and hot spring waters, respectively, are noted (Figure 6A-6C). This correlation implies that the Eu abundance is roughly related to the proportion of deep brine (Figure 6A) and is different from other REEs (Figure 5A-5C). As is graphically expressed in Figure 4, the five hot spring waters are depleted in REEs compared to 'Kinsen' and have decreased Cl contents, although the decrease in Eu abundance is less than that in other REEs. Figure 6 also shows that Eu behaves in correlation with Ca and Sr, suggesting the possible involvement of plagioclase, which may selectively buffer Eu among the REEs [23]. This possibility is examined subsequently.

Discussion

Origin and process of Eu-anomaly

In previous studies of the geochemical characterization of slab-derived fluid beneath volcanic arcs, no Eu-anomaly has been reported for slab-fluids as a possible source of the deep brine [24]. The estimated composition of slab-fluid from the Philippine Sea slab generally shows a smooth pattern with downward sloping toward HREEs [25]. The slab-derived fluid exhibits variable REE abundances depending on the temperature of dehydration. With slab dehydration at lower temperatures beneath the fore-arc region, including the Arima area, REEs in the slab-fluid exhibit significantly lower abundances due to the large temperature dependence of the partition coefficient between fluid and residual solids [26-28]. As a result of dehydration, the REE pattern
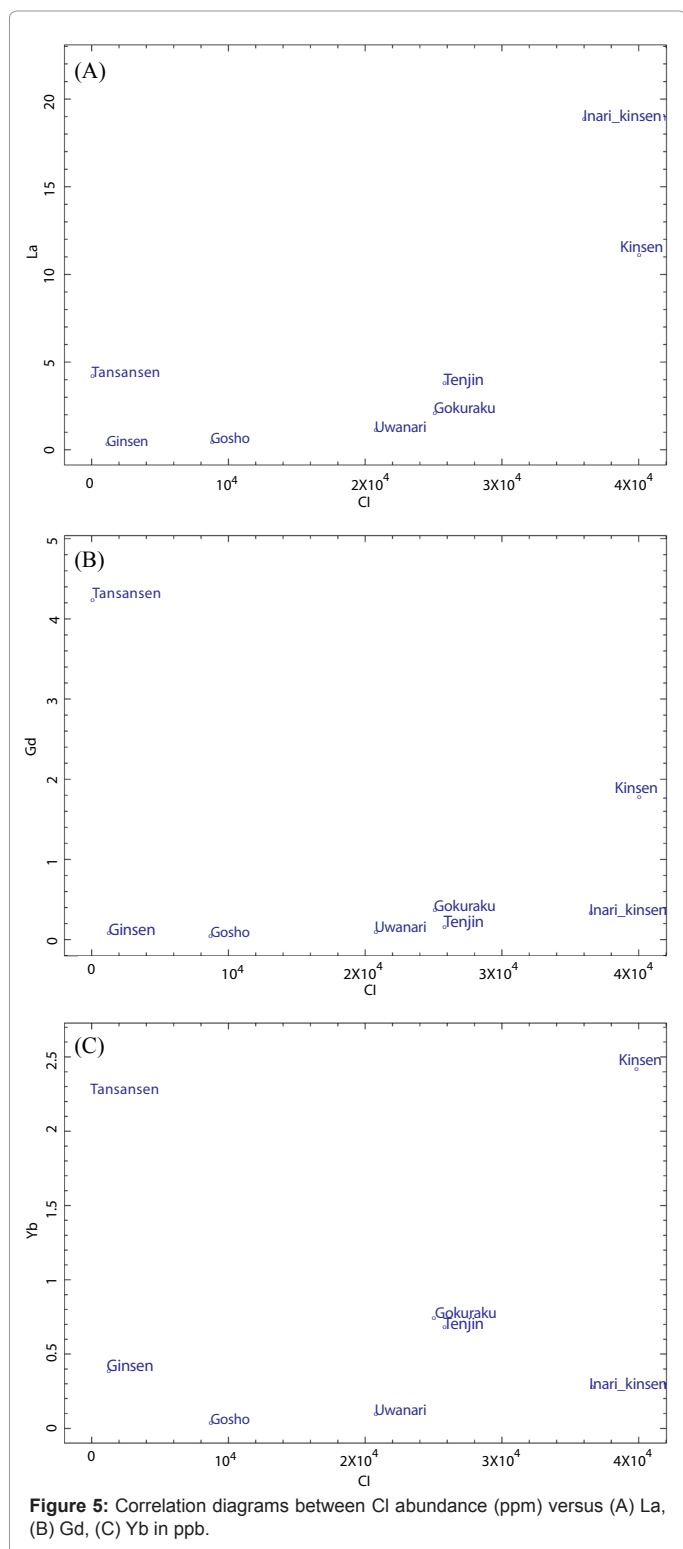
in a slab-derived fluid shows a smooth and slight convex-down pattern. Therefore, the positive Eu-anomaly observed for 'Kinsen' and other hot spring waters (Figure 4) is attributed to processes that occurred during their ascent from depth, likely at a shallow level when the deep brine encountered near-surface water under oxidizing conditions.

In this case with oxidizing conditions within a relatively shallow aquifer, if the temperature is decreased from the original high temperature state up to 500°C, REEs can coprecipitate as a form of $Ln(OH)_3$ with Fe oxyhydroxide [9,10]. The chemical reaction of Ln, involving slab-derived fluid and near-surface (e.g., meteoric) water as reactants with solid precipitates as reaction products, is expressed as $Ln^{3+}_{(aq)} + 3H_2O_{(aq)} \leftrightarrows Ln(OH)_{3(ss)} + 3H^+_{(aq)}$, where (aq) and (ss) denote aqueous solution and solid solution, respectively. It is also suggested that during this precipitation process, Eu in the spring waters has to be retained relative to the other REEs, resulting in a positive Eu-anomaly. If plagioclase abundant in Eu with a positive anomaly exists in the matrix of an aquifer, it may supply Eu for buffering, as is observed. Therefore, the low REE abundance with a strong positive Eu-anomaly in Figure 4, as is observed for 'Gokuraku', 'Gosho', 'Inari-Kinsen', 'Tenjin' and 'Uwanari' hot springs, is interpreted to be a result of overlapping effects associated with elution of Eu and precipitation of other REEs under relatively oxidized conditions. The difference in these five hot springs and 'Kinsen' could be attributed to the degree of the reaction progress due to retention time within the aquifer, although these springs may share a common deep brine.

Conversely, the negative Eu-anomaly observed in 'Tansansen' may have developed under relatively reductive conditions in presence of feldspar such as by reaction with surrounding rocks having negative Eu-anomalies such as Rokko granite or that by (organic) C in the sedimentary rocks exposed in this area [4,23]. The relationship between Eu behavior and other REEs concerning 'Tansansen' is discussed subsequently.
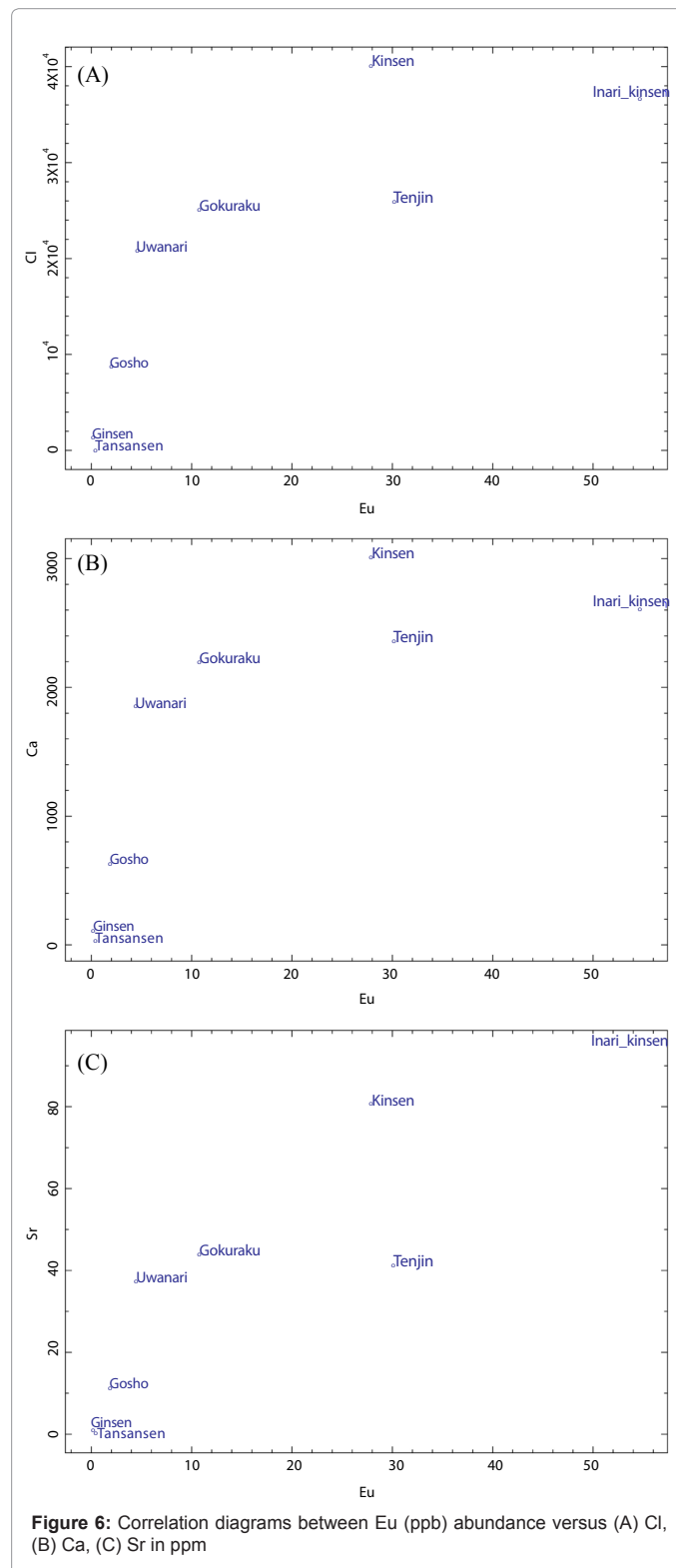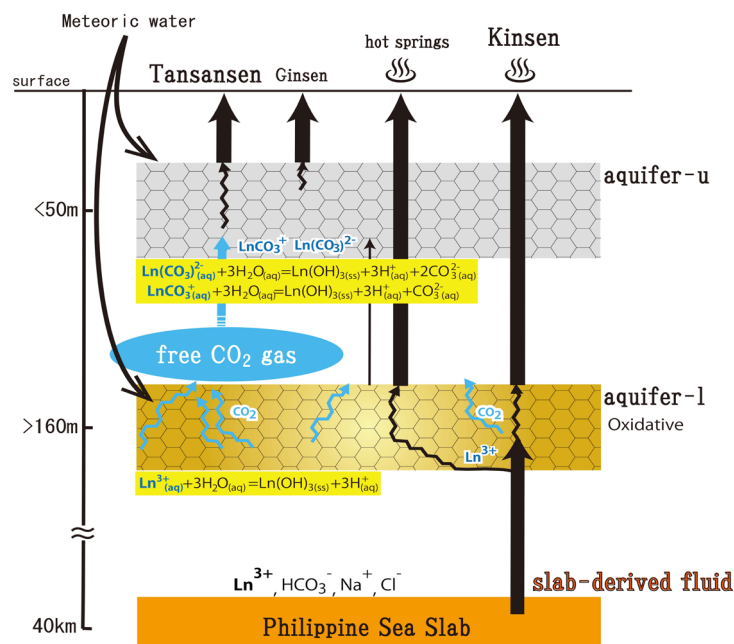
Behavior of REEs

Despite the negative Eu-anomaly and the lowest Cl content of the spring waters analyzed in this study, 'Tansansen' shows high REE concentrations and a flat pattern, except for Eu. The flat REE pattern is notably distinct from those of other Arima spring waters, basement igneous rocks, and river water [1,25] in particular, 'Tansansen' has higher HREE contents. This feature can be explained by the existence of CO_2 gas and carbonate species in aqueous fluid [26-28]. The gas-saturated fluid exhibits solubility of $Ln^{3+}(CO_3)_2^-$ approximately four times higher at 1 atm [29,30]. In addition, REEs are more preferentially partitioned into fluid than Fe oxyhydroxide with increasing $NaHCO_3$ concentration, and the dominant REE(III) species in aqueous solutions changes from $REE^{3+}_{(aq)}$ to $REECO3^+_{(aq)}$ and then to $REE(CO_3)_2^-_{(aq)}$. This transition decreases Racah (E1 and E3) parameters for 4f electron repulsion of REEs and rapidly modifies the REE abundances in aqueous

Figure 5: Correlation diagrams between Cl abundance (ppm) versus (A) La, (B) Gd, (C) Yb in ppb.

flat pattern with a weaker positive Eu-anomaly compared than that in hot spring waters (type (iv) in Figure 4), suggesting a carbonate effect similar to 'Tansansen' but to a lesser extent. It is also noted that the cold springs are derived from a shallow aquifer seated at ~40 m in depth, yet their REE concentrations are significantly higher (up to 1000 times) than those in nearby river waters (Figure 5) [7]. This result indicates

Figure 6: Correlation diagrams between Eu (ppb) abundance versus (A) Cl, (B) Ca, (C) Sr in ppm

solution from a relatively low level with a significant tetrad effect pattern to higher concentrations with a smooth pattern, depending on the carbonate abundance [9]. Therefore, highly carbonated water such as 'Tansansen' may have a high and flat REE pattern caused by reaction with solids. The 'Ginsen' cold spring, which has δ^{18}O and δD close to the meteoric water line (Figure 3A), also exhibits a relatively

Figure 7: Geochemical evolution model for spring waters in the studied area. Meteoric aquifer-l is the same as lower meteoric aquifer (aq-l) in the main text. Meteoric aquifer-u is the same as upper meteoric aquifer (aq-u) in the text. The abbreviations used in the equations, (aq) and (ss), denote aqueous solution and solid solution, respectively.

that a significant uptake of REEs has occurred even during a shallow cycling of near-surface water.

Comprehensive model for Arima spring waters

Based on the observations and arguments discussed thus far, we propose a model for shallow-level chemical evolution of Arima spring waters, as shown in Figure 7. At least two types of meteoric aquifers occur beneath the study area. One correspond to lower aquifers (aq-l) seated deeper than 160 m, and the other represents upper aquifers (aq-u) shallower than ~40 m [7,8]. The slab-derived fluid dehydrated at a minimum temperature of 500°C from subducting PHS migrates upward and enters the upper aquifer, where it is mixed with meteoric waters to variable extents and is cooled to ~130°C [8]. Within the lower aquifer, the precipitation reaction, discussed above, occurs to induce degassing of CO_2 and He. The separated gas phase migrates upward and enters the upper aquifer to produce highly carbonated meteoric water with high $^3He/^4He$ ratios [2,7]. The precipitates remove REEs from the aqueous solution to variable extents, whereas the solution reacts with feldspar with a strong positive Eu-anomaly to produce the geochemical characteristics of 'Gokuraku', 'Gosho', 'Inari-Kinsen', 'Tenjin', and 'Uwanari' hot springs (Figures 4 and 7). The differences among these five hot springs may represent the degrees of such reactions reflecting retention time in aq-l.

Within aq-u, the host rock is thought to be composed of silicic igneous rocks with high REE contents with negative Eu-anomalies such as the Rokko granite or rhyolite exposed in this area [23]. When the CO_2-bearing gas phase that separates from aq-l dissolves into aq-u, dissolution of the REE elements from the rock matrix to the aqueous solution is enhanced, fingerprinting the Eu-negative anomaly of the host rocks. These processes within aq-u produced 'Tansansen' and 'Ginsen', the latter showing lesser dissolution. The 'Kinsen' hot spring water is nearly upwelled directly from the subducted slab through both

meteoric aquifers, even though a small degree of interaction is inferred from the weak positive Eu-anomaly, as shown in Figure 7.

In order to test this scenario, knowledge of the composition and reaction ratio of the meteoric waters and the host rocks is required. On the basis of these data, the model calculates qualitative and quantitative revisions. In any case, the abundances and patterns of REEs in the spring waters appear to provide unique and invaluable information on the chemical evolution of the deep brine at relatively shallow levels, which has been obtained by neither major solute elements nor isotopic compositions. The REE compositions will be useful for investigating such shallow chemical processes of other springs, especially cold–hot spring association, because the nature of the deep brine is clarified through removal of the shallow effects.

Conclusion

In addition to examining the major solute elements and isotopic compositions including $\delta^{18}O$–δD, He, and Sr–Nd–Pb systematics reported in previous studies, we have performed REE analyses for both hot and cold spring waters in the Arima area. We have shown that the simple binary mixing between the deep brine and meteoric water inferred from the previous studies cannot explain the REE variations. We have identified the following four distinct REE patterns according to isotope composition and major solute element and gas compositions: (i) high REE content with a flat pattern and negative Eu-anomaly, having the lowest $\delta^{18}O$ and δD isotopic ratios with abundant CO_2 gas and the highest He isotopic ratio; (ii) high REE content with a slightly convex-down pattern and positive Eu-anomaly, having the highest $\delta^{18}O$ and δD isotopic ratios with a high He isotopic ratio; (iii) lower REE content with a strong convex-down pattern and a positive Eu-anomaly, having lower $\delta^{18}O$–δD isotopic ratio with lower He isotopic ratios; and (iv) a slightly convex-down pattern with a moderately

positive Eu-anomaly and a negative Ce-anomaly, having similar $\delta^{18}O$, δD, and He isotopic ratios as that in type (i).

We have presented the following model to explain the shallow-level chemical evolution of the deep brine resulting in distinct features of Arima spring waters. Two sources are present for REEs. The first is deep brine likely originating from the subducted Philippine Sea slab, and the other is basement crustal rocks serving as aquifers. The deep brine encounters meteoric water at the lower aquifer under relatively oxidizing conditions, in which the formed precipitates remove REEs from the solution and a CO_2-bearing gas phase is generated. In the upper meteoric aquifer, the gas from the lower aquifer dissolves in the meteoric water and enhances the solubility of REEs from the host rocks into the solution. This process produces cold spring waters with a flat REE pattern of relatively high concentrations. This information obtained by REE analysis will be useful for understanding the shallow geochemical processes for other spring waters that have not been identified by major solute or isotopic studies.

Acknowledgements

References

1. Nakamura H, Fujita Y, Nakai S, Yokoyama T, Iwamori H (2014) Rare earth elements and Sr–Nd–Pb isotopic analyses of the Arima hot spring waters, Southwest Japan: implications for origin of the Arima-type brine. J Geol Geosci 3: 161.

2. Matsubaya O, Sakai H, Kusachi I, Satake H (1973) Hydrogen and oxygen isotopic ratios and major element chemistry of Japanese thermal water systems. Geochem J 7: 123-151.

3. Tanaka K, Koizumi M, Seki R, Ikeda N (1984) Geochemical study of Arima hot-spring waters, Hyogo, 408 Japan, by means of tritium and deuterium. Geochem J 18: 173-180.

4. Masuda H, Sakai H, Chiba H, Tasurumaki M (1985) Geochemical characteristics of Na-Ca-Cl-HCO_3 type waters in Arima and its vicinity in the western Kinki distinct, Japan. Geochem J 19: 149-162.

5. Nagao K, Takaoka N, Matsubaya O (1981) Rare gas isotopic compositions in natural gases in Japan. Earth Planet Sci Lett 53: 175-188.

6. Sano Y, Wakita H (1985) Geographical distribution of $^3He/^4He$ ratios in Japan – implications for arc tectonics and incipient magmatism. J Geophys Res 90: 8729-8741.

7. Kusuda C, Iwamori H, Nakamura H, Kazahaya K, Morikawa N (2014) Arima hot spring waters as a deep-seated brine from subducting slab. Earth Planets Space 66: 119.

8. Kozuki J (1962) Studies of Arima Spa. Nippon Shoin, Tokyo (in Japanese).

9. Ohta A, Kawabe I (2000) Rare earth element partitioning between Fe oxyhydroxide precipitates and aqueous NaCl solutions doped with $NaHCO_3$: Determinations of rare earth element complexation constants with carbonate ions. Geochem J 34: 439-454.

10. Ohta A, Kawabe I (2000) Theoretical study of tetrad effects observed in REE distribution coefficients between marine Fe-Mn deposit and deep seawater, and in REE (III)-carbonate complexation constants. Geochem J 34: 455-473.

11. Mitchell TM, Ben-Zion Y, Shimamoto T (2011) Pulverized fault rocks and damage asymmetry along the Arima-Takatsuki Tectonic Line, Japan. Earth Planet Sci Lett 308: 284-297.

12. Maruyama T, Lin A (2002) Active strike-slip faulting history inferred from offsets of topographic features and basement rocks: a case study of the Arima-Takatsuki Tectonic Line, southwest Japan. Tectonophysics 344: 81-101.

13. Sangawa A (1978) Fault topography and quaternary faulting along the middle and eastern parts of the Arima-Takatsuki tectonic line, Kinki district, central Japan. Geographical Review of Japan 51: 760-775 (Japanese with English abstract).

14. Nakajima J, Hasegawa A (2007) Subduction of the Philippine Sea plate beneath southwestern Japan: Slab geometry and its relationship to arc magmatism. J Geophys Res 112: B08306.

15. Hirose F, Nakajima J, Hasegawa A (2008) Three-dimensional seismic velocity structure and configuration of the Philippine Sea slab in southwestern Japan estimated by double-difference tomography. J Geophys Res 113: B09315.

16. Iwamori H (2007) Transportation of H_2O beneath the Japan arcs and its implications for global water circulation. Chem Geol 239: 182-198.

17. Fujita K, Kasama T (1983) Geological map. Geological Survey of Japan, National Institute of Advanced Industrial Science and Technology, Japan.

18. Arai T, Tainosho Y (2004) Lithologic variation and plutonic history of the Late Cretaceous granitoids in the Rokko Mountains, southwest Japan. J Geol Soc Jap 110: 452-462 (Japanese with English abstract).

19. Kazahaya K, Takahashi M, Yasuhara M, Nishio Y, Inamura A, et al. (2014). Spatial distribution and feature of slab-related deep-seated fluid in SW Japan. Journal of Japanese Association of Hydrological Science 44: 3-16 (in Japanese).

20. Uemoto M (2008) Principles and practices of ICP emission and ICP mass spectrometry, Ohmsha, Tokyo (in Japanese).

21. Chang Q, Shibata T, Shinotsuka K, Yoshikawa M, Tatsumi Y (2003) Precise determination of trace elements in geological standard rocks using inductively coupled plasma mass spectrometry (ICP-MS). Frontier Research on Earth Evolution 1: 357-362.

22. Teranishi K, Isomura K, Yano M, Chayama K, Fujiwara S, et al. (2003) Measurement of distribution of rare earth elements in Arima-type springs using preconcentration with chelating resin/ICP-MS. Bunseki Kagaku 52: 289-296.

23. Terakado Y, Fujitani T (1995) Significance of iron and cobalt partitioning between plagioclase and biotite for problems concerning the Eu^{2+}/Eu^{3+} ratio, europium anomaly, and magnetite-/ilmenite-series designation for granitic rocks from the Inner zone of southwestern Japan. Geochim Cosmochim Acta 59: 2689-2699.

24. Nakamura H, Iwamori H (2009) Contribution of slab-fluid in arc magmas beneath the Japan arcs. Gondwana Res 16: 431-445.

25. Nakamura H, Iwamori H (2013) Generation of adakites in a cold subduction zone due to double subducting plates. Contrib Mineral Petrol 165: 1107-1134.

26. Pandler C, Hermann A, Arculus R, Mavrogenes J (2003) Redistribution of trace elements during prograde metamorphism from lawsonite blueschist to eclogite facies; implications for deep subduction-zone processes. Contrib Mineral Petrol 146: 205-222.

27. Kessel R, Schmidt MW, Ulmer P, Pettke T (2005) Trace element signature of subduction-zone fluids, melts and supercritical liquids at 120–180 km depth. Nature 437: 724-727.

28. Kimura JI, Hacker BR, van Keken PE, Kawabata H, Yoshida T, et al. (2009) Arc Basalt Simulator version 2, a simulation for slab dehydration and fluid-fluxed mantle melting for arc basalts: Modeling scheme and application. Geochem Geophys Geosyst 10: Q09004.

29. Michard A, Beaucaire G, Michard G (1987) Uranium and rare earth elements in CO_2-rich waters from Vals-les-Bains (France). Geochim Cosmochim Acta 51: 901-909.

30. Johannesson KH, Stentzenbach KJ, Hodge F (1997) Rare earth elements as geochemical tracers of regional groundwater mixing. Geochim Cosmochim Acta 61: 3605-3618.